Fuel Processing Technology 177 (2018) 6–15

Contents lists available at ScienceDirect

Fuel Processing Technology

journal homepage: www.elsevier.com/locate/fuproc

Research article

Selective ring opening of decalin on Rh-Pd/SiO_2-Al_2O_3 bifunctional systems: Catalytic performance and deactivation

Silvana A. D'Ippolito[a], Laurence Pirault-Roy[b], Catherine Especel[b,*], Florence Epron[b], Carlos L. Pieck[a]

[a] Instituto de Investigaciones en Catálisis y Petroquímica (INCAPE) (FIQ-UNL, CONICET), Colectora Ruta Nac. N° 168 km 0, Paraje El Pozo, CP 3000 Santa Fe, Argentina
[b] Institut de Chimie des Milieux et des Matériaux de Poitiers (IC2MP), Université de Poitiers, UMR 7285 CNRS, 4 rue Michel Brunet, 86073 Poitiers Cedex 9, France

ARTICLE INFO

Keywords:
Decalin
Ring opening
Bifunctional catalysts
Bimetallic catalysts
Rh-Pd

ABSTRACT

Ring opening of decalin was studied using Rh-Pd(x) catalysts supported on SiO_2-Al_2O_3, prepared by coimpregnation with a variable total metallic content (x = 1, 1.5 and 2 wt%) while maintaining constant the Rh/Pd atomic ratio (equal to 1). The catalytic performances of these bimetallic systems were compared to those of monometallic Pd and Rh (1 wt%) catalysts. Bimetallic Rh-Pd(x) catalysts were unable to achieve decalin conversion and ring opening selectivity as high as those obtained using the Rh catalyst (~71 and ~67%, respectively, after 6 h reaction time). The principal cause was the reduction of the hydrogenolytic activity and acidity caused by the combination of Pd and Rh. In the case of the bimetallic Rh-Pd(x) samples, an increase in the metal content favored the formation of dehydrogenated products, reduced cracking (by reducing the concentration of strong acid sites) and increased coke deposition during decalin ring opening. Conversely, the Rh catalyst showed less deactivation since its efficient hydrogenolytic character eliminates coke precursors.

1. Introduction

The increase in diesel consumption drives researchers to study the reactions of Selective Ring Opening (SRO) to convert aromatic or naphthenic compounds into linear paraffins, improving the cetane index [1]. The interest to increase the economic value of the Light Cycle Oil (LCO) using SRO is confirmed by the numerous patents referred to the subject [2–9]. The SRO mechanism consists in a saturation of the aromatic rings, followed by isomerization and ring opening reactions, even cracking [10–13]. Ring opening is considered to proceed *via* a direct route (over the metallic sites), or *via* an indirect one where ring contraction products are opened by a bifunctional mechanism. For such a reaction, metallic dispersion and acidity of the catalysts are key parameters affecting their performance. Metals from Group VIII (Rh, Ru, Ir, Pt and Pd) were reported as efficient in terms of activity and selectivity to ring opening when dispersed over acid supports [14–18]. The catalysts used in SRO of decalin and tetralin (model molecules for the LCO) can be classified into: (i) monofunctional solids, mainly zeolites H-Y, H-Beta and H-mordenite [14,19] leading to low yields to ring opening products and high amounts of cracking products, (ii) noble metals on non-acid supports [11,20,21], (iii) bifunctional catalysts characterized by the presence of acid and metal sites. In the latter case, the first publications referred mostly to systems consisting of zeolites and noble metals such as platinum and iridium [10,14,22–29]. The bifunctional catalysts with noble metals supported on HY zeolite (high acidity) could lead depending on the operation conditions to deactivation by coke formation due to diffusion limitations. For this reason, noble metal catalysts supported on mesoporous oxides were studied [12,30–33].

It has been proposed that the ring opening reaction in presence of bifunctional catalysts begins with the ring contraction from 6 to 5 carbon atoms over acid sites, followed by easier opening of the 5-membered cycle due to the hydrogenolytic activity of the metal [20,34,35]. Selectivity to ring opening and ring contraction products can be tuned according to the ratio between acid and metallic sites, which can be adjusted by varying the nature of the support, the composition of the metallic phase (mono or bimetallic function, metal content and metal particle size) [13]. The importance of acid function on the SRO reaction was reported by several studies [36–38].

In previous works, we reported that the acidity and the Rh/Pd content ratio of Rh-Pd/SiO_2-Al_2O_3 catalysts have a strong influence on the activity and selectivity for the decalin ring opening reaction [39–41]. As the deactivation is a very important factor to be considered in the selection of the best catalysts, we decided to revisit the Rh-Pd catalysts supported on SiO_2-Al_2O_3. The objective of the present study is to evaluate the effect of the metallic and acid functions of Rh-Pd

* Corresponding author.
E-mail address: catherine.especel@univ-poitiers.fr (C. Especel).

https://doi.org/10.1016/j.fuproc.2018.04.008
Received 5 January 2018; Received in revised form 4 April 2018; Accepted 8 April 2018

catalysts supported on SiO_2-Al_2O_3 on both their performances for the selective ring opening of decalin and their resistance to deactivation process. It is important to note that these types of bifunctional catalysts are proposed as a replacement of noble metals supported on zeolites, since these last suffer from excessive cracking and deactivation. Moreover, Taillades-Jacquin et al. reported the use of Rh-Pd catalysts supported on mesoporous aluminosilicate in industrial processes aiming to improve diesel quality by hydrogenation and ring-opening of aromatic components and to increase the thioresistance [31].

2. Experimental

2.1. Catalyst preparation

Commercial SiO_2-Al_2O_3 supplied by SASOL (SIRAL 60 noted S60 containing 57.4 and 42.6 wt% of SiO_2 and Al_2O_3, respectively) with a specific surface area of 489 $m^2\,g^{-1}$ was used as support. The calcined support (4 h, 450 °C, air, 60 $cm^3\,min^{-1}$) was left for 1 h in HCl solution (0.2 mol L^{-1}) before impregnation, the added solution volume being of 1.5 $cm^3\,g_{cat}{}^{-1}$. The necessary amounts of $PdCl_2$ and $RhCl_3$ precursor salts were added to synthesize the Pd/S60 and Rh/S60 monometallic catalysts containing both 1 wt% metal content, and three Rh-Pd/S60 bimetallic catalysts with 1, 1.5 and 2 wt% as total metal content, keeping a constant Rh/Pd atomic ratio equal to 1. The suspension was gently agitated for 1 h, and then dried at 70 °C until a dry powder was obtained. The catalysts were further dried at 120 °C overnight. Finally, they were calcined (air, 60 $cm^3\,min^{-1}$, 300 °C, 4 h) and reduced (H_2, 60 $cm^3\,min^{-1}$, 500 °C, 4 h). The bimetallic catalysts were named Rh-Pd (x)/S60, x corresponding to the total metal loading (wt%).

2.2. Pyridine temperature programmed desorption (pyridine TPD)

The acidic function of the bifunctional catalysts was characterized by pyridine TPD. 100 mg of catalyst were impregnated at room temperature with an excess of pyridine, and left in a fume hood to obtain a dry powder by evaporation. A quartz reactor was loaded with the powder and the weakly adsorbed pyridine was eliminated by flowing N_2 (40 mL min^{-1}, 110 °C, 1 h). Then, the temperature was increased up to 750 °C at 10 °C min^{-1} while the amount of pyridine at the reactor outlet was measured by gas chromatography equipped with a FID detector.

2.3. Transmission electron microscopy

The morphology of the catalysts was evaluated by transmission electron microscopy (TEM) on a JEOL 2100 instrument, coupled with energy dispersive X-ray spectroscopy (EDX), according to an experimental procedure previously described [40]. By exploitation of the images with the ImageJ software, mean surface diameters ($d = \Sigma(n_i d_i^3)/\Sigma(n_i d_i^2)$) were determined by measuring at least 600 particles for each analyzed sample, and the metal dispersion was calculated considering spherical particles.

2.4. Dynamic CO chemisorption

This technique was used to measure metallic particle dispersion. It was carried out in a dynamic adsorption equipment, by injecting calibrated CO pulses in the presence of a continuous flow of an inert gas over the sample. First, 75 mg of samples previously reduced after their preparation were reduced again under H_2 at 500 °C (10 °C min^{-1}) for 1 h. Then, N_2 was circulated for 1 h at 500 °C to eliminate all traces of adsorbed H_2. Finally, the samples were cooled to room temperature under N_2 and CO pulses of 0.6 μmol were injected with a 2 min frequency until saturation.

2.5. Cyclopentane hydrogenolysis

The model reaction of cyclopentane (CP) hydrogenolysis was used to evaluate the hydrogenolysis activity of the metal function. The reaction was carried out for 2 h in a fixed bed reactor under atmospheric pressure at 225 °C, using 80 mg of catalyst, and following experimental conditions previously reported [33]. Before the reaction the catalyst was reduced at 500 °C during 1 h (H_2, 36 $cm^3\,min^{-1}$).

2.6. Cyclohexane dehydrogenation

The metallic function of the catalysts was also characterized by its activity for the cyclohexane (CH) dehydrogenation performed at 270 °C (with 20 mg of catalyst prereduced *in situ*). The experimental protocol used for this model reaction has been previously described [42].

2.7. Decalin ring opening

An autoclave stainless steel reactor was used to carry out the reaction at 350 °C under a total and constant pressure of 3 MPa (H_2 atmosphere), an agitator speed of 1360 rpm, a decalin volume of 25 cm^3 and 1 g of catalyst. Decalin containing 37.5% of the cis isomer was used as reactant. Before decalin reaction, the catalyst was reduced *in situ* under hydrogen (1 h, 350 °C, atmospheric pressure). The initial reaction time was considered when the agitation was turn-on (immediately after the reaction pressure and temperature were achieved). Diffusion limitations due to mass transfer were negligible (calculated Weisz-Prater module $\Phi = 0.06 \ll 1$). At the end of the reaction run (after 6 h), the reactor temperature was cooled down until room temperature and samplings of liquid mixtures were analyzed in a Shimadzu 2014 gas chromatograph with a Phenomenex ZB-5 capillary column and a FID. The gas phase was analyzed revealing a small C_1-C_4 fraction in agreement with the results reported by Kubička et al. [10]. Product identification was performed through GC-MS in a Saturn 2000 mass spectrometer coupled to a Varian 3800 gas chromatograph using the same GC column.

2.8. Differential scanning calorimetry (DSC)

The analysis of the used catalysts (after 6 h of decalin ring opening reaction) was performed on a Mettler Toledo DSC821e Differential Scanning Calorimeter equipment. The coked catalysts (approximately 10 mg) were heated under air flow (50 $cm^3\,min^{-1}$) from 30 °C until 600 °C (10 °C min^{-1}).

2.9. Temperature programmed oxidation (TPO)

The carbon deposited on the used catalysts was analyzed by TPO experiments, according to the experimental protocol described elsewhere [33].

3. Results and discussion

The total acidity and distribution of the acid strength of the mono and bimetallic catalysts supported on S60 were determined by pyridine TPD. The values obtained for each catalyst (and bare S60 support) are gathered in Table 1, as well as the residual chlorine content present on the activated samples. It was previously reported that the total acidity of the support (S60) was 1559 μmol of pyridine per gram of catalyst, the impregnation with 0.2 mol L^{-1} solution of HCl produced an increase of the total acidity up to 1970 μmol of pyridine per gram of catalyst [32]. This fact points out the importance of the presence of chlorine species on the acidity. In a previous work, we found that the total acidity of the alumina is increased almost three times by the chlorine addition [43]. It was stated that the total acidity of the catalysts is increased by the Cl^- species [44] which can be incorporated by the metal precursors or by

Table 1
Total acidity and acid strength distribution as determined by pyridine (Py) TPD for monometallic and bimetallic Rh-Pd(x)/S60 catalysts (x = 1, 1.5 and 2 wt%).

Catalyst	Chlorine, wt%	Total acidity, μmol Py g_{cat}^{-1}	Acid site concentration, μmol Py g_{cat}^{-1}		
			Weak (T < 300 °C)	Moderate (300 < T < 500 °C)	Strong (T > 500 °C)
S60	0.00	1559	251	1161	147
Pd	1.03	2210	44	884	1282
Rh-Pd(1)	0.85	2028	71	1450	507
Rh-Pd(1.5)	1.04	2736	109	2299	328
Rh-Pd(2)	1.21	2145	43	1952	150
Rh	1.03	2957	44	1671	1242

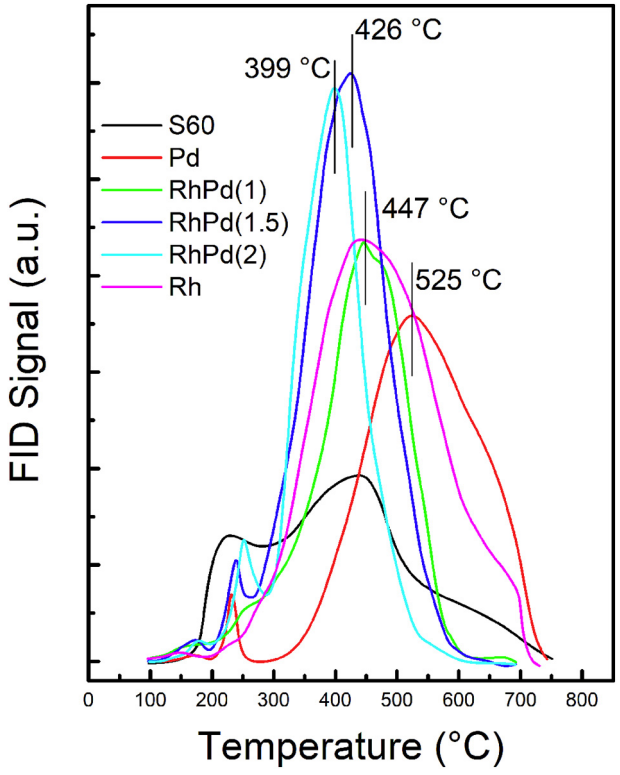

Fig. 1. TPD pyridine profiles obtained for monometallic and bimetallic Rh-Pd (x)/S60 catalysts (x = 1, 1.5 and 2 wt%).

the HCl used as competitor during preparation protocol to produce a homogeneous metal distribution on the support.

It can be seen in Fig. 1 that the incorporation of metal (Rh or Pd) and chlorine produces a major increase of the total acidity and changes on the acid strength distribution. Acid sites with medium and strong strengths are created while the weak acid sites are decreased. Fig. 1 shows that the maximum temperature of the main peak obtained for the three Rh-Pd(x)/S60 samples shifts to lower temperatures (from 447 °C to 399 °C) while increasing the total metallic content (from 1 to 2 wt%). Similar results were previously observed on SIRAL 40 support impregnated with Rh and Pd [39]. This tendency reflects the decrease in the amount of strong acid sites corresponding to pyridine quantity desorbed above 500 °C, as reported in Table 1. Excepting the Pd/S60 catalyst, which presents mostly strong acid sites, the other studied samples possess mostly acid sites of moderate strength (associated to pyridine desorption from 300 to 500 °C). It is important to note that the total acidity of the bimetallic Rh-Pd(x)/S60 catalysts is below that of the Rh/S60 catalyst, the following order being obtained: Rh-Pd(1)/S60 < Rh-Pd(2)/S60 < Pd/S60 < Rh-Pd (1.5)/S60 < Rh/S60.

The electronic interactions of the metal particles with the support can change the support acidity. Several authors reported the same behavior, *i.e.*, changes in the acid strength distribution and in the total acidity of the support by metal addition, with in most of the cases a decrease of the strength and total amount of acid sites [10,45–50]. In their review [50], Stakheev and Kustov explained that the strength of acid sites involved in the metal-support interaction becomes weaker as a result of the electron density transfer from (or onto) the metal. However, there are some contradictory results as for example those of Santi et al. [37] reporting that the metal addition increases the acidity.

By comparing the values of chlorine content and of total acidity reported in Table 1, it can be concluded that there is not a correlation between each other. The support acidity could be due to two opposite effects: i) chlorine entities increase the support acidity by polarizing the bonds of the Al cations with which they are linked [[51] and the references therein], ii) the strength of acid sites involved in the metal-support interaction becomes weaker as a result of the electron density transfer from (or onto) the metal [50].

The morphology of the catalysts was evaluated by transmission electron microscopy (TEM) coupled with energy dispersive X-ray spectroscopy (EDX), in order to observe the accurate localization of the metallic particles, to analyze their chemical nature and to estimate their average size and dispersion. Figs. 2 and 3 display representative TEM images and particle size distributions for the monometallic and bimetallic catalysts, respectively. The mean particle diameters and metal dispersions are reported in Table 2. For both monometallic catalysts and the Rh-Pd(x)/S60 catalysts with x = 1 and 1.5 wt%, the metallic phase is homogeneously dispersed on the support with particle sizes comprised mainly between 1.5 and 4.0 nm. In the case of the Rh-Pd(2)/S60 sample, a certain heterogeneity appears regarding the distribution of the particles on the support and their average size, with a larger average particle size (5.75 nm). Furthermore, EDX analysis performed on the three bimetallic catalysts reveals the presence of particles composed of both Pd and Rh species, suggesting the existence of a bimetallic interaction.

Table 2 shows that both monometallic catalysts display virtually the same values of CO chemisorption, in line with the average particle size and dispersion determined from the TEM pictures. In the case of Rh-Pd (x)/S60 catalysts, the CO/M value decreases at increasing metal loads in agreement with the evolution of the average particle size determined by TEM analysis. In order to measure the hydrogenolysis metallic activity, the model reaction of cyclopentane hydrogenolysis was performed, knowing it is promoted by large particles exhibiting metallic ensembles [52]. The cyclopentane conversions and CP TOF values reveal that the Rh monometallic catalyst presents a higher hydrogenolytic activity compared to Pd one (factor 2 between the respective activities, Table 2). For the bimetallic catalysts, CP conversions are between those of the monometallic catalysts, but slightly increase with the total metallic content, in agreement with the decrease in metallic dispersion [53]. Finally, the Rh-Pd(x)/S60 bimetallic catalysts display CP TOF values closer to that of the Pd/S60 sample than that of the Rh/S60 one. This tendency could be due to a geometric effect, *i.e.* to the presence of Pd atoms blocking Rh ensembles, or electronic effect resulting from a charge transfer from Pd to Rh, in accordance to their electronic affinities (0.56 eV for Pd, and 1.14 eV for Rh). Superficial enrichment of the bimetallic ensembles by Pd atoms could also occur [54].

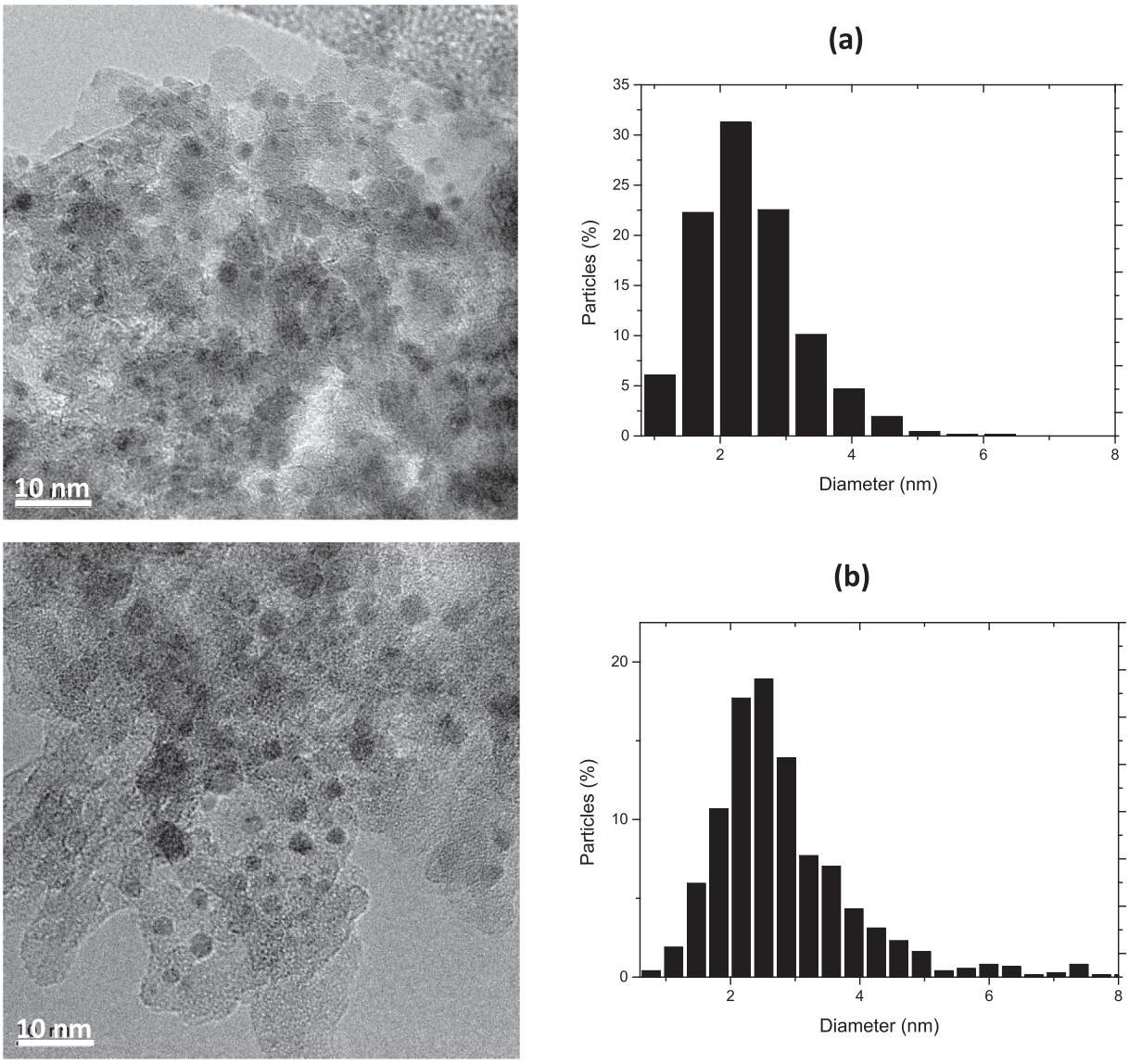

Fig. 2. TEM pictures and size distribution of monometallic catalysts: (a) Pd/S60, (b) Rh/S60.

The large spectrum of decalin reaction products (over 200 compounds) was classified as: cracking products (CR, C_1-C_9); ring opening products (RO, C_{10}); ring contraction products (RC); dehydrogenation products (DP) (naphthalene and heavy dehydrogenation products) [22]. To correlate the reaction products with the catalyst properties, it is necessary to consider the reaction mechanisms proposed in the literature for decalin ring opening taking into account the specificities of the studied catalysts. Arribas and Martínez [55] by considering the strong hydrogenating activity of Pt proposed a monomolecular mechanism as the most probable for the hydrocracking of methylnaphthalene on bifunctional Pt/USY catalysts. According to this mechanism, the aromatic rings of methylnaphthalene can be hydrogenated on Pt sites followed by isomerization (contraction) of the saturated C_6 rings to C_5 rings and subsequent ring opening, the latter two steps being catalyzed mainly by the Brønsted acid sites of the bifunctional Pt/USY catalysts. A similar reaction mechanism was proposed by Monteiro et al. [56] for the decalin hydroconversion on Pt/zeolite catalysts. It is important to point out that both reaction mechanisms do not consider the hydrogenolysis activity of the metal.

There are several differences between our studied catalysts and Pt/zeolite catalysts: i) Pt exhibits a very high hydrogenation/dehydrogenation activity compared to Rh and Pd, ii) Pt presents a low hydrogenolysis activity compared to Rh, iii) zeolites possess more stronger acid sites than SIRAL 60. Taking into account the higher hydrogenolysis activity of Rh and the contribution of the acid sites on the reaction mechanism, we consider that the ring opening of decalin begins with the ring contraction from 6 to 5 carbon atoms over acid sites, followed by easier opening of the 5-membered cycle due to the hydrogenolysis activity of the metal. This mechanism is widely accepted [20,34,35].

From Table 3, it is possible to see that bimetallic catalysts are unable to surpass Rh/S60 catalyst in conversion and selectivity to RO. These behaviors can result from the weak hydrogenolytic activity of Pd and its dilution effect on the Rh ensembles as observed previously for the CP hydrogenolysis. The higher yield to RO products obtained with the Rh/S60 catalyst relative to the Pd/S60 one can be attributed to the higher total acidity and hydrogenolytic activity of this first, in accordance with a bifunctional decalin ring opening mechanism where the first reaction step is the ring contraction from 6 to 5 carbon atoms [18,34]. These five-membered rings are further easily opened over Rh. In the case of the Rh-Pd(x)/S60 bimetallic catalysts, at increasing metallic loads, the yield to cracking products (CR) reduces, while the yield to

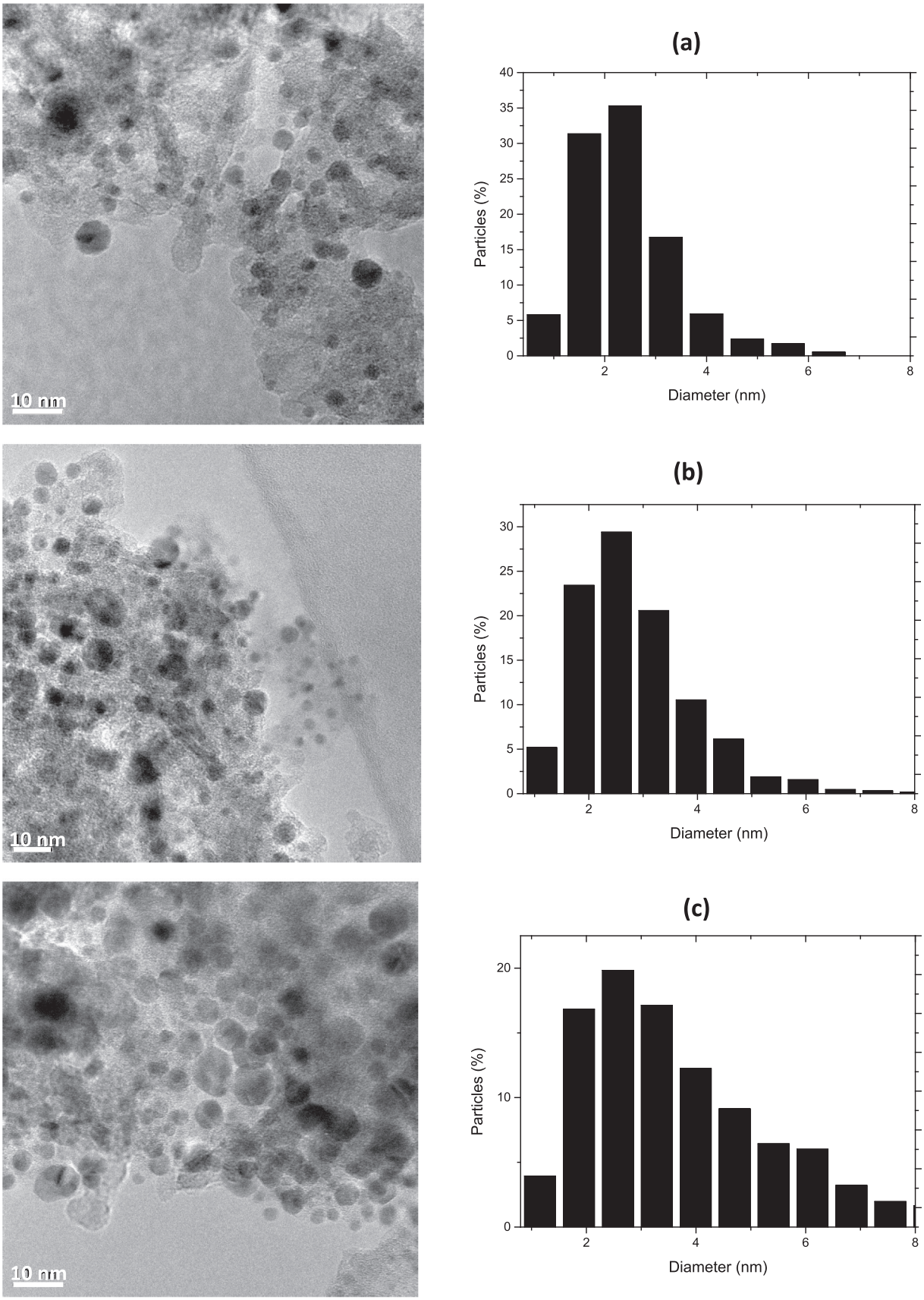

Fig. 3. TEM pictures and size distribution of bimetallic Rh-Pd(x)/S60 catalysts: (a) x = 1 wt%, (b) x = 1.5 wt%, (c) x = 2 wt%.

Table 2
Particle diameter (d) and metal dispersion (D) estimated from TEM pictures, CO chemisorption values, initial conversion (extrapolated to zero reaction time) and TOF value for cyclopentane (CP) hydrogenolysis and cychohexane (CH) dehydrogenation obtained for monometallic (1 wt%) and bimetallic Rh-Pd(x)/S60 catalysts (x = 1, 1.5 and 2 wt%).

Catalyst/S60	d, nm	D, %	CO/M, %	CP conversion, %	CP TOF[a], s^{-1}	CH conversion, %	CH TOF[a], s^{-1}
Pd	3.89	28.5	0.30	22.0	0.105	3.5	0.277
Rh-Pd(1)	3.52	31.2	0.37	29.3	0.111	4.5	0.286
Rh-Pd(1.5)	3.96	27.8	0.33	31.7	0.090	6.0	0.281
Rh-Pd(2)	5.75	19.1	0.26	42.6	0.115	6.0	0.281
Rh	4.05	26.9	0.31	49.3	0.219	2.9	0.217

[a] TOF values calculated from the reaction rate determined at zero reaction time (extrapolated value) and the CO/M values considering a stoichiometry of adsorbed CO per surface metal atom equal to 1 [68,69].

dehydrogenated products (DP) increases (unwanted products due to their poor cetane index).

Fig. 4(a) and (b) show the decalin conversion obtained for each catalyst as a function of their strong acid sites quantity determined from pyridine TPD (Table 1), and of the hydrogenolysis metallic activity expressed as cyclopentane conversion (Table 2), respectively. The decalin conversion increases as strong acid sites and hydrogenolysis metallic activity increase, with however in both figures one point without correlation with the general tendency. On one hand, Fig. 4(a) shows that the Pd/S60 catalyst with a high amount of strong acid sites and a low hydrogenolytic activity leads to a lower decalin conversion. On the other hand, in Fig. 4(b), the Rh-Pd(2)/S60 catalyst with a few quantity of strong acid sites and a high cyclopentane conversion displays a lower decalin conversion. The particular behavior of these two samples points out that an optimal balance between both sites (acidic and metallic) is necessary to obtain efficient catalysts for the decalin conversion.

In the same way as Fig. 4, Fig. 5(a) and (b) show that both functions (metal and acid) are needed to obtain a high yield to RO products, since a high amount of strong acid sites and a low hydrogenolysis metallic activity (case of the Pd/S60 sample), as well as a high hydrogenolysis metallic activity and a low amount of strong acid sites (case of the Rh-Pd(2)/S60 sample) induce a low yield to RO products. According to the catalytic performances of the catalyst series gathered in Table 3, the selectivity to RO products seems to increase with the decalin conversion. Initially, the reactant feed contains 37.5% of the cis one, with a trans/cis ratio of 1.63. At the end of the reaction, this ratio is even more largely in favor of the trans isomer with around 10 times more of trans isomer than of cis one (Table 3). Previous studies have already shown that cis-decalin is easier to open than trans-decalin, which is mostly converted into cracking products [14]. Finally, Fig. 6 indicates that the RO selectivity is correlated with the percentage of cis-decalin remaining at the end of reaction: the lower is the cis-decalin percentage, the higher is the RO selectivity.

According to the results displayed in Fig. 7, the cracking products

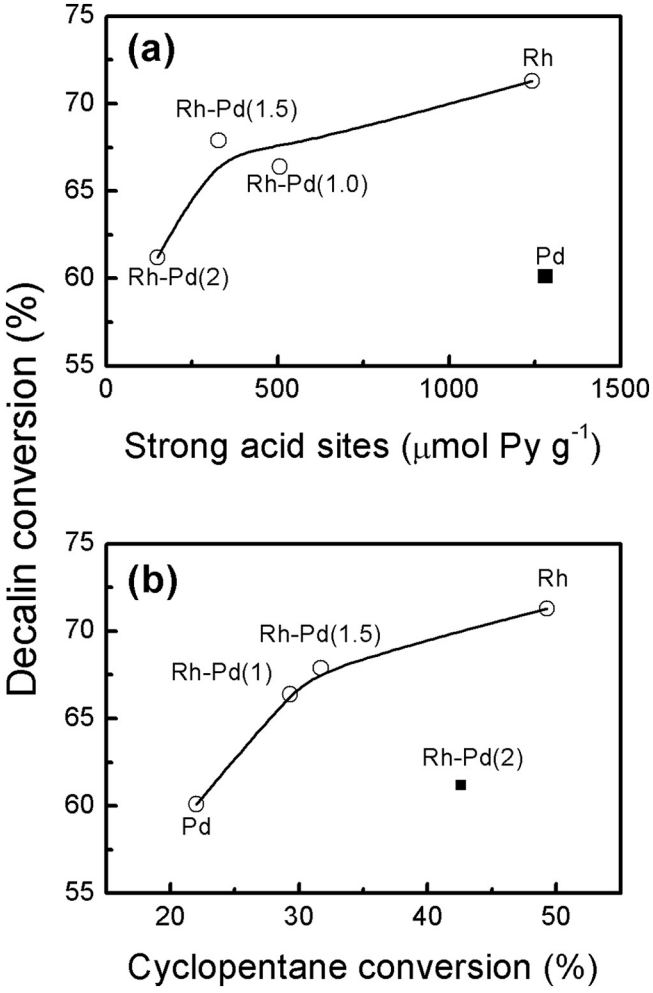

Fig. 4. Decalin conversion (after 6 h reaction time) as a function of (a) the strong acid sites concentration and (b) the cyclopentane conversion obtained for monometallic and bimetallic Rh-Pd(x)/S60 catalysts (x = 1, 1.5 and 2 wt%).

yield increases with the quantity of strong acid sites (Brønsted and/or Lewis, only the global acidity being evaluated in this work) in agreement with the fact that the cracking reactions are catalyzed by the sites of strong acidity [57]. It was found that the removal of strong acid sites by addition of potassium into iridium catalysts supported on USY zeolite reduces the formation of cracking products in hydrotreating of LCO [58]. Again, the Pd/S60 catalyst has an anomalous behavior with a low CR yield and a high amount of strong acid sites. The low CR yield of the Pd catalyst despite of its important quantity of strong acid sites could be linked to the high DP yield obtained with this sample (Table 3). The aromatic compounds produced by dehydrogenation on the metal function are then more difficult to crack by the acid function [59,60]. Compared to Rh/S60, Pd/S60 catalyst possesses effectively a slightly

Table 3
Decalin conversion; yield to cracking products (CR), ring contraction products (RC), ring opening products (RO) and dehydrogenation products (DP); RO selectivity; trans and cis decalin concentration obtained for monometallic and bimetallic Rh-Pd(x)/S60 catalysts (x = 1, 1.5 and 2 wt%) after 6 h reaction time.

Catalyst/S60	Conversion, %	Yield, %				RO selectivity, %	Decalin, %	
		CR	RC	RO	DP		Trans	Cis
Pd	60.1	1.9	9.3	34.8	14.1	57.9	36.9	3.0
Rh-Pd(1)	66.4	5.4	12.1	41.6	7.3	62.7	31.1	2.5
Rh-Pd(1.5)	67.9	3.2	13.0	43.5	8.2	64.1	29.5	2.6
Rh-Pd(2)	61.2	1.3	6.6	33.4	19.9	54.6	35.2	3.6
Rh	71.3	7.0	11.7	47.4	5.2	66.5	26.8	1.9

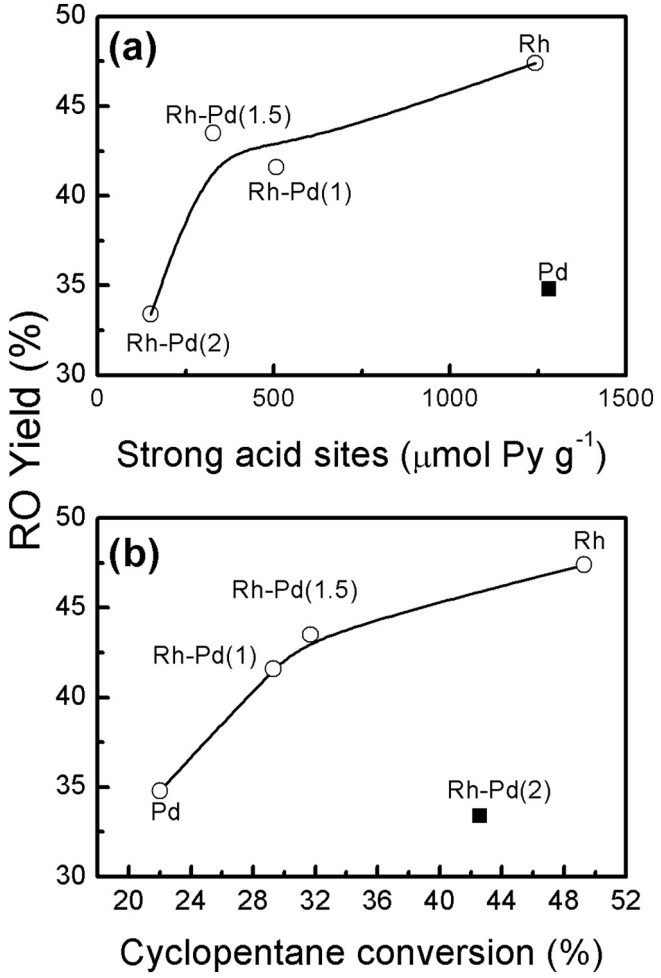

Fig. 5. RO yield (after 6 h reaction time) as a function of (a) the strong acid sites concentration and (b) the cyclopentane conversion obtained for monometallic and bimetallic Rh-Pd(x)/S60 catalysts (x = 1, 1.5 and 2 wt%).

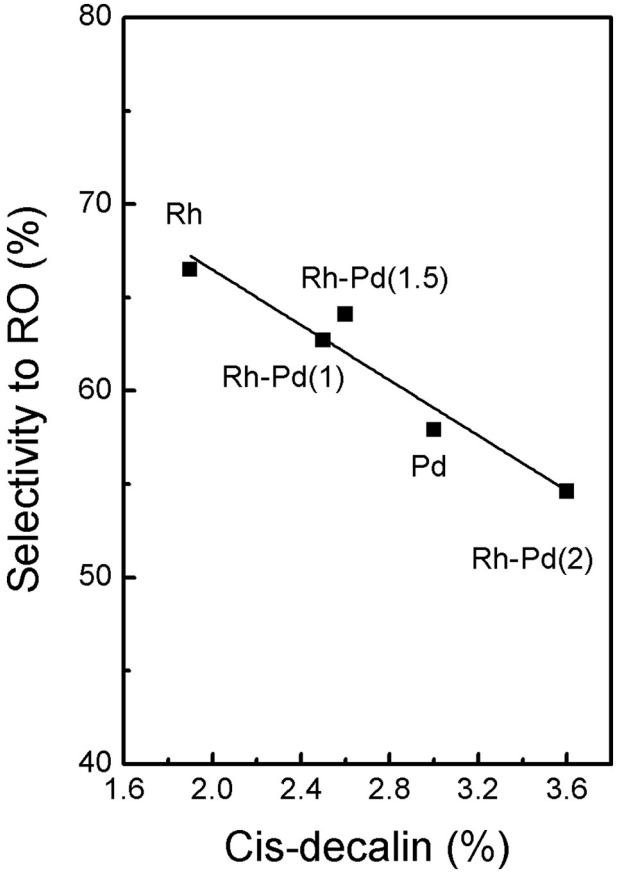

Fig. 6. Selectivity to RO products as a function of percentage of cis-decalin obtained after 6 h reaction time for monometallic and bimetallic Rh-Pd(x)/S60 catalysts (x = 1, 1.5 and 2 wt%).

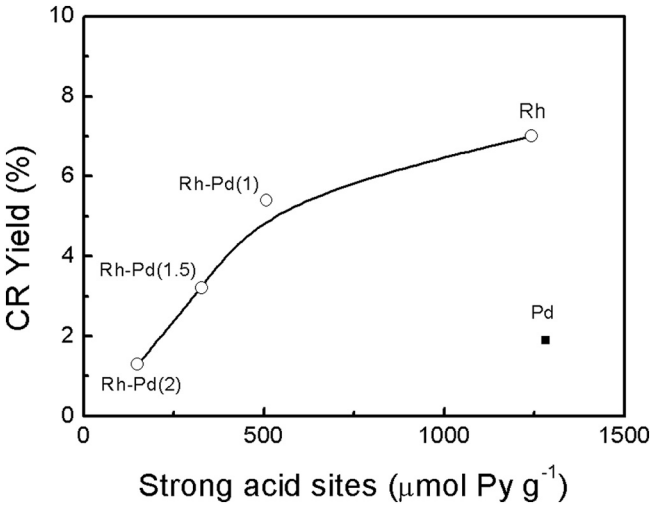

Fig. 7. CR yield (after 6 h reaction time) as a function of the strong acid sites concentration obtained for monometallic and bimetallic Rh-Pd(x)/S60 catalysts (x = 1, 1.5 and 2 wt%).

higher dehydrogenating activity as revealed by the model reaction of CH dehydrogenation while its hydrogenolytic activity (measured by CP hydrogenolysis) is around twice lower (Table 2) [61,62]. Consequently, the Pd/S60 metal function could favor the formation of dehydrogenation products rather than that of ring opening products. Therefore, considering DP products are formed by a route parallel to the RC, RO and CR reactions, another explanation could be advanced: the formation of heavier DP products (such as polyaromatics) would favor the formation of coke on acid sites decreasing cracking reactions. Among the studied bimetallic samples, RhPd(2) catalyst exhibits the highest CH conversion and also the highest yield of DP compounds. It is expected that RhPd(2) catalyst produces lower amounts of dehydrogenated product due to its high hydrogenolysis activity. Probably, the high amounts of dehydrogenated products formed on the sample lead to a coke deposition involving a decrease of the CR and RC yields (reactions promoted by acid sites), and then of the RO yield.

It is interesting to analyze more in depth the CR products distribution to determine if the cracking products are formed by a hydrocracking or hydrogenolysis process. Haas et al. and Santi et al. [21,37] found that the selectivity to cracking products has a "M"-type C-number distribution (maximum selectivities for C_4 and C_6 and lower selectivities to C_2, C_3, C_5, C_7 and C_8) when the reaction is controlled by the acid function. The reaction mechanism implies the classical bifunctional hydrocracking *via* carbocations. On the other hand, when the cracking products are produced by hydrogenolysis on the metal function, the cracking products distribution shows a "hammock"-type distribution (high selectivity to C_9 and C_1 and lower selectivity to C_3 to C_7). The main cracking products obtained are: 2-methylbutane, hexane, 2,3-dimethylpentane, 3-methylpentane, methylcyclopentane (abundant), propylcyclopentane, 2-methylpropylcyclopentane, 1,1-dimethylcyclopentane, cyclohexane, methylcyclohexane, propylcyclohexane, cis 1-ethyl-2-methylcyclohexane, trans 1-ethyl-4-methylcyclohexane, 1-ethyl-3-methylcyclohexane, 1,1,4-trimethylcyclohexane. Taking into

Table 4
Yield to C_5-C_8 and C_9 products, and C_9/C_5-C_8 ratio of the cracking products (CR) fraction.

Catalyst/S60	Yield, %		C_9/C_5-C_8
	C_5-C_8	C_9	
Pd	0.87	1.03	1.18
RhPd(1)	3.13	2.27	0.72
RhPd(1.5)	1.08	2.12	1.97
RhPd(2)	0.37	0.93	2.51
Rh	3.68	3.32	0.90

account that C_5-C_8 are produced by hydrocracking on the acid function and C_9 are formed on the metal by hydrogenolysis, the C_9/C_5-C_8 ratio of the cracking products fraction can be used as a parameter to determine the balance of the metal and acid functions. The obtained values are gathered in Table 4, as well as the respective yields to C_5-C_8 and C_9 products. As expected, in the case of the bimetallic catalysts, the C_9/C_5-C_8 ratio increases with the hydrogenolysis activity for CP conversion (reported in Table 2). In spite of the fact that monometallic Rh catalyst displays the highest hydrogenolysis activity for CP conversion, similar yields to cracking (C_5-C_8) and hydrogenolysis (C_9) products are observed during decalin conversion. This could be due to the fact this catalyst has also the highest amount of strong acid sites (Table 1). In conclusion, the results presented in Table 4 show that the cracking products obtained during decalin conversion are formed by hydrogenolysis on metal sites and cracking on acid sites.

Fig. 8(a) shows the DSC profiles obtained from burning coke deposited on the catalysts during decalin reaction. The temperature at which the combustion occurs is related to the nature of the coke (soft or graphitic) and its location (on metallic sites or on support). These parameters have a bigger impact on the stability of the catalysts than the amount of carbon deposit [57]. The coke content and distribution were determined by TPO analysis, the obtained profiles being presented in Fig. 8(b). The peaks observed at low temperatures (below 250 °C) on the TPO profiles can be assigned to coke deposited over or near metallic particles that catalyzed the combustion, while the second burning zone is attributed to coke localized over the support [63]. Maldonado-Hódar et al. related that at increasing coke contents, the carbon deposit becomes more stable and DSC peaks are then shifted to higher temperatures [64]. This behavior is also observed for the three studied bimetallic catalysts on the basis of the obtained DSC profiles (Fig. 8(a)) and the carbon contents determined at the end of the SRO reaction of decalin (Fig. 9). Nonetheless, peaks at higher temperatures could also be due to diffusional limitations induced by pore blocking by polyaromatic compounds [65]. With the studied catalysts, it is important to note that DSC peaks are all located below 550 °C, corresponding to the presence of amorphous coke. The chemical reactivity of this kind of coke is high due to structural defects and it can be eliminated easier than others [66].

From Fig. 8(b), we can conclude that most of the coke is deposited over the support. According to the literature, coke deposition over metallic sites is limited if the metal particles are small enough [63,67]. Effectively in the case of the Rh-Pd(x)/S60 catalysts, the area under the TPO curves until 250 °C increases at decreasing metallic dispersion values. The low coke deposition over the Rh/S60 monometallic catalyst and notably on the metallic function of this sample is a consequence of the high hydrogenolytic activity of Rh favoring the destruction of coke precursors.

Fig. 9a shows a direct proportionality between the carbon content of the used catalysts and the yield to dehydrogenated products obtained during decalin conversion. Dehydrogenated products have been proposed as coke formation precursors, formed on the metallic sites and then polymerized over the acid sites of the support [67]. Moreover, Fig. 9b exhibits a reverse correlation between CR yield and carbon content showing that (i) at high hydrogenolytic activity (as well as in the presence of numerous strong acid sites in the case of Rh/S60 sample) the coke precursors can be destroyed, or (ii) CR products are more numerous on catalysts with lower coke content due to a lower formation of DP products, and therefore the acid function is less deactivated. Finally, the catalysts exhibiting the highest deactivation by carbon deposit (Pd/S60 and Rh-Pd(2)/S60) are those leading to the lowest decalin conversions and selectivities to RO products.

4. Conclusions

This work was devoted to the study of monometallic and bimetallic Rh-Pd catalysts supported on SiO_2-Al_2O_3 (SIRAL 60) for the selective ring opening reaction of decalin. The objective was to appreciate the influence on the catalytic properties of the nature of the metallic function constituted of 1 wt% Pd, 1 wt% Rh or x wt% Rh-Pd (with x, the total metal loading equal to 1, 1.5 or 2 while keeping the Rh/Pd atomic

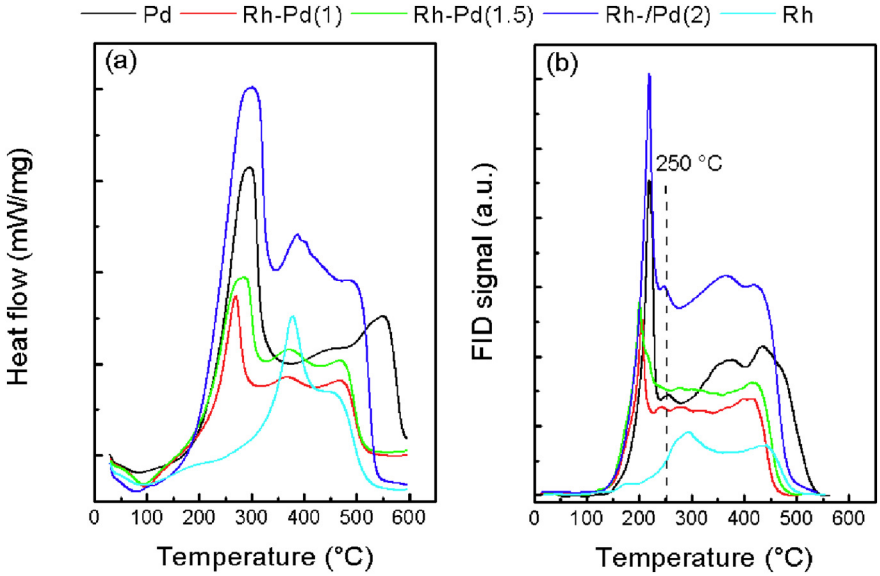

Fig. 8. (a) DSC profiles and (b) TPO profiles obtained for the used monometallic and bimetallic Rh-Pd(x)/S60 catalysts (x = 1, 1.5 and 2 wt%) after 6 h of decalin reaction.

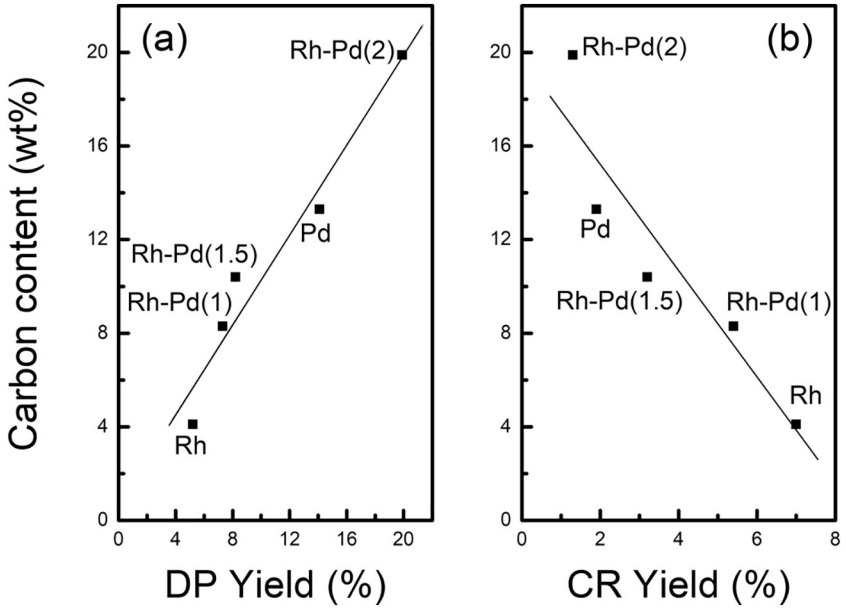

Fig. 9. Carbon content determined from TPO profiles *vs* (a) DP yield and (b) CR yield obtained for the monometallic and bimetallic Rh-Pd(x)/S60 catalysts (x = 1, 1.5 and 2 wt%) after 6 h of decalin reaction.

ratio equal to 1) deposited on the acid support. The catalytic properties were discussed in terms of decalin conversion, selectivity to various products (*i.e.* ring opening (RO) products, ring contraction (RC) products, cracking (CR) products, and dehydrogenation products (DP)), and resistance to coke deposit. The decalin transformation was considered to proceed *via* a bifunctional mechanism: the transformation of decalin begins with the ring contraction from 6 to 5 carbon atoms over acid sites, followed by easier opening of the 5-membered cycle due to the hydrogenolysis activity of the metal. It was found that cracking products are formed both by hydrogenolysis on the metal function and by hydrocracking on the acid sites.

The obtained results reveal that the bimetallic Rh-Pd(x)/S60 catalysts are unable to achieve the decalin conversion and selectivity to RO observed with Rh/S60 monometallic catalyst. Compared to the monometallic Rh/S60 sample, the combination of Rh and Pd generates a decrease in the overall hydrogenolytic activity and in the number of strong acid sites. Moreover, with the increase in the metallic content of the bimetallic Rh-Pd(x)/S60 catalysts, a fall in the dispersion of the metallic particles and in the quantity of strong acid sites is observed, decreasing the CR yield, but enhancing the amount of dehydrogenated products and coke deposition rates during the decalin ring opening reaction. Finally, among the studied catalysts, the monometallic Rh/S60 sample presents the lowest deactivation rate due to its hydrogenolytic character that favors the destruction of coke precursors.

References

[1] R.C. Santana, P.T. Do, M. Santikunaporn, W.E. Alvarez, J.D. Taylor, E.L. Sughrue, D.E. Resasco, Fuel 85 (2006) 643–656.
[2] G.B. McVicker, M.S. Touvelle, C.W. Hudson, D.E.W. Vaughan, M. Daage, S. Hantzer, D.P. Klein, E.S. Ellis, B.R. Cook, O.C. Feeley, US Patent 5,763,731 (1998).
[3] Ying-Yen P. Tsao, T.J. Huang, P.J. Angevine, US Patent 6,500,329 (2002).
[4] W.C. Baird, J.G. Chen, G.B. McVicker, US Patent 6,623,626 (2003).
[5] I. Galperin, Deng-Y Jan, M.J. McCall, J.A. Kocal, L.B. Galperin, US Patent 7,405,177 (2008).
[6] R. Giardino, V. Calemma, U. Cornaro, US Patent 8,236,171 (2012).
[7] H. Ta Dindi, G. Thanh, US Patent 9,212,323 (2015).
[8] N. Semagina, X. Yin, J. Shen, K. Loganathan, US Patent 9,040,449 (2015).
[9] H. Dindi, L.E. Murillo, A.H. Pulley, US Patent 9,139,782 (2015).
[10] D. Kubička, N. Kumar, P. Maeki-Arvela, M. Tiitta, V. Niemi, H. Karhu, T. Salmi, D.Y. Murzin, J. Catal. 227 (2004) 313–327.
[11] G.B. McVicker, M. Daage, M.S. Touvelle, C.W. Hudson, D.P. Klein, W.C. Baird Jr., B.R. Cook, J.G. Chen, S. Hantzer, D.E.W. Vaughan, E.S. Ellis, O.C. Feely, J. Catal. 210 (2002) 137–148.
[12] K.C. Mouli, V. Sundaramurthy, A.K. Dalai, Z. Ring, Appl. Catal. A 321 (2007) 17–26.
[13] S. Nassreddine, L. Massin, M. Aouine, C. Geantet, L. Piccolo, J. Catal. 278 (2011) 253–265.
[14] M. Santikunaporn, J.E. Herrera, S. Jongpatiwut, D.E. Resasco, W.E. Alvarez, E.L. Sughrue, J. Catal. 228 (2004) 100–113.
[15] J.L. Carter, J.A. Cusumano, J.H. Sinfelt, J. Catal. 20 (1971) 223–229.
[16] C.G. Walter, B. Coq, F. Figueras, M. Boulet, Appl. Catal. A 133 (1995) 95–102.
[17] A.H. Alzaid, K.J. Smith, Appl. Catal. A Gen. 450 (2013) 243–252.
[18] K. Arve, P. Mäki-Arvela, K. Eränen, M. Tiitta, T. Salmi, D.Yu. Murzin, Chem. Eng. J. 238 (2014) 3–8.
[19] D. Kubička, N. Kumar, P. Mäki-Arvela, M. Tiitta, V. Niemi, T. Salmi, D.Y. Murzin, J. Catal. 222 (2004) 65–79.
[20] R. Moraes, K. Thomas, S. Thomas, S. Van Donk, G. Grasso, J.-P. Gilson, M. Houalla, J. Catal. 286 (2012) 62–77.
[21] A. Haas, S. Rabl, M. Ferrari, V. Calemma, J. Weitkamp, Appl. Catal. A Gen. 425–426 (2012) 97–109.
[22] S.A. D'Ippolito, L.B. Gutierrez, C.L. Pieck, Appl. Catal. A Gen. 445–446 (2012) 195–203.
[23] S.A. D'Ippolito, L.B. Gutierrez, C.R. Vera, C.L. Pieck, Appl. Catal. A Gen. 452 (2013) 48–56.
[24] M.A. Arribas, A. Corma, M.J. Díaz-CabaÇas, A. Martínez, Appl. Catal. A 273 (2004) 277–286.
[25] N. Kumar, D. Kubička, A.L. Garay, P. Mäki-Arvela, T. Heikkilä, T. Salmi, D.Y. Murzin, Top. Catal. 52 (2009) 380–386.
[26] D. Kubička, T. Salmi, M. Tiitta, D.Y. Murzin, Fuel 88 (2009) 366–373.
[27] K. Chandra Mouli, V. Sundaramurthy, A.K. Dalai, J. Mol. Catal. A Chem. 304 (2009) 77–84.
[28] K. Chandra Mouli, A.K. Dalai, Appl. Catal. A Gen. 364 (2009) 80–86.
[29] D. Kubička, M. Kangas, N. Kumar, M. Tiitta, M. Lindblad, D.Y. Murzin, Top. Catal. 53 (2010) 1438–1445.
[30] A. Infantes-Molina, J. Mérida-Robles, E. Rodríguez-Castellón, J.L.G. Fierro, A. Jiménez-López, Appl. Catal. B 73 (2007) 180–192.
[31] M. Taillades-Jacquin, D.J. Jones, J. Rozière, R. Moreno-Tost, A. Jiménez-López, S. Albertazzi, A. Vaccari, L. Storaro, M. Lenarda, J.-M. Trejo-Menayo, Appl. Catal. A Gen. 340 (2008) 257–264.
[32] S.A. D'Ippolito, A.D. Ballarini, C.L. Pieck, Energy Fuel 31 (2017) 5461–5471.
[33] S.A. D'Ippolito, L. Pirault-Roy, C. Especel, F. Epron, C.L. Pieck, RSC Adv. 7 (2017) 46803–46811.
[34] H. Du, C. Fairbridge, H. Yang, Z. Ring, Appl. Catal. A Gen. 294 (2005) 1–21.
[35] A. Galadima, O. Muraza, Fuel 181 (2016) 618–629.
[36] S. Rabl, A. Haas, D. Santi, C. Flego, M. Ferrari, V. Calemma, J. Weitkamp, Appl. Catal. A Gen. 400 (2011) 131–141.
[37] D. Santi, T. Holl, V. Calemma, J. Weitkamp, Appl. Catal. A Gen. 455 (2013) 46–57.
[38] V. Calemma, M. Ferrari, S. Rabl, J. Weitkamp, Fuel 111 (2013) 763–770.
[39] S.A. D'Ippolito, C. Especel, L. Vivier, F. Epron, C.L. Pieck, Appl. Catal. A Gen. 469 (2014) 532–540.
[40] S.A. D'Ippolito, C. Especel, L. Vivier, S. Pronier, F. Epron, C.L. Pieck, J. Mol, Catal. A Chemical 398 (2015) 203–214.
[41] S.A. D'Ippolito, C. Especel, F. Epron, C.L. Pieck, Fuel Process. Technol. 140 (2015) 180–187.
[42] P. Samoila, F. Epron, P. Marécot, C. Especel, Appl. Catal. A Gen. 462–463 (2013) 207–219.

[43] L.S. Carvalho, C.L. Pieck, M.C. Rangel, N.S. Fígoli, C.R. Vera, J.M. Parera, Appl. Catal. A Gen. 269 (2004) 105–116.
[44] B.C. Gates, J.R. Katzer, G.C.A. Schuit, Chemistry of Catalytic Processes, McGraw-Hill, New York, 1979, pp. 184–324.
[45] J.I. Villegas, D. Kubička, H. Karhu, H. Österholm, N. Kumar, T. Salmi, D.Yu. Murzin, J. Mol, Catal. A Chem. 264 (2007) 192–201.
[46] D. Kubička, N. Kumar, T. Venäläinen, H. Karhu, I. Kubičková, H. Österholm, D.Yu. Murzin, J. Phys. Chem. B 110 (2006) 4937–4946.
[47] A.K. Aboul-Gheit, S.M. Abodoul-Fotouh, N.A.K. Abodoul-Gheit, Appl. Catal. A Gen. 292 (2005) 144–153.
[48] A.K. Aboul-Gheit, S.M. Abodoul-Fotouh, S.M. Abdel-Hamid, N.A.K. Abodoul-Gheit, J. Mol. Catal. A Chem. 245 (2006) 167–177.
[49] V. Nieminen, M. Kangas, T. Salmi, D.Yu. Murzin, Ind. Eng. Chem. Res. 44 (2005) 471–484.
[50] A.Yu. Stakheev, L.M. Kustov, Appl. Catal. A Gen. 188 (1999) 3–35.
[51] J.R. Regalbuto, G.J. Antos, G.J. Antos, A.M. Aitani (Eds.), Catalytic Naphtha Reforming, 2nd ed., Marcel Dekker, New York, 2004, pp. 141–198 (Chapter 5).
[52] A. Roberti, V. Ponec, W.M.H. Sachtler, J. Catal. 28 (1973) 381–390.
[53] B. Biloen, J. Helle, H. Verbeek, F. Dautzembverg, W. Sachtler, J. Catal. 63 (1980) 112–118.
[54] P. Araya, J.P. Berrios, Appl. Catal. A 92 (1992) 17–27.
[55] M.A. Arribas, A. Martínez, Appl. Catal. A 230 (2002) 203–217.
[56] C.A.A. Monteiro, D. Costa, J.L. Zotin, D. Cardoso, Fuel 160 (2015) 71–79.
[57] J.M. Parera, N.S. Fígoli, G.J. Antos, A.M. Aitani, J.M. Parera (Eds.), Catalytic Naphtha Reforming: Science and Technology, Marcel Dekker, New York, 1995(Chap 3).
[58] D.P. Upare, R. Nageswara Rao, S. Yoon, C. Wee Lee, Res. Chem. Intermed. 37 (2011) 1293–1303.
[59] J.H. Gary, G.E. Handwerk, Petroleum refining Technology and Economics, 4th edition, Marcel-Dekker Inc., New York-Basel, 2001, pp. 108–109.
[60] W.A. Cruse, D.R. Stevens, Chemical Technology of Petroleum, 3rd edition, Mc Graw-Hill Book Company, New York, 1960, pp. 375–387.
[61] Y. Wang, N. Shah, F.E. Huggins, G.P. Huffman, Energy Fuel 20 (2006) 2612–2615.
[62] K. Yukawa, T. Fujii, Y. Saito, J. Chem. Soc. Chem. Commun. 21 (1991) 1548–1549.
[63] J. Barbier, G. Corro, Y. Zhang, J.P. Bournonville, J.P. Franck, Appl. Catal. 13 (1985) 245–255.
[64] F.J. Maldonado-Hódar, M.F. Ribeiro, J.M. Silva, A.P. Antunes, F.R. Ribeiro, J. Catal. 178 (1998) 1–13.
[65] P. Magnoux, M. Guisnet, Zeolites 9 (1989) 329–335.
[66] C. Wang, N. Sun, N. Zhao, W. Wei, Y. Sun, C. Sun, H. Liu, C.E. Snape, Fuel 143 (2015) 527–535.
[67] J. Barbier, Appl. Catal. 23 (1986) 225–243.
[68] F.P. Bouxin, X. Zhang, I.N. Kings, A.F. Lee, M.J.H. Simmons, K. Wilson, S.D. Jackson, Appl. Catal. A Gen. 539 (2017) 29–37.
[69] G. Prelazzi, M. Cerboni, G. Leofanti, J. Catal. 181 (1999) 73–79.